

**Mid-infrared spectroscopic assessment of nanotoxicity in Gram-negative vs. Gram-positive bacteria**

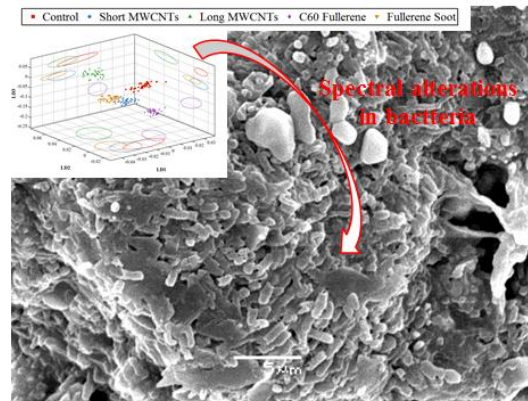
*Kelly A. Heys<sup>1,2</sup>, Matthew J. Riding<sup>1</sup>, Rebecca J. Strong<sup>1</sup>, Richard F. Shore<sup>2</sup>, M. Glória Pereira<sup>2</sup>, Kevin C. Jones<sup>1</sup>, Kirk T. Semple<sup>1</sup>, Francis L. Martin<sup>1</sup>*

<sup>1</sup>Centre for Biophotonics, Lancaster Environment Centre, Lancaster University, Bailrigg, Lancaster LA1 4YQ, UK

<sup>2</sup>Centre of Ecology and Hydrology, Lancaster University, Bailrigg, Lancaster LA1 4YQ, UK

**Corresponding author:** Prof. Francis L Martin, Centre for Biophotonics, LEC, Lancaster University, Lancaster LA1 4YQ, UK; Tel.: +44 (0)1524 510206; Email: [f.martin@lancaster.ac.uk](mailto:f.martin@lancaster.ac.uk)

## ToC graphic



Vibrational spectroscopy provides a spectral fingerprint identifying the effects of carbon-based nanoparticles in bacterial cells.

## ABSTRACT

Nanoparticles appear to induce toxic effects through a variety of mechanisms including generation of reactive oxygen species (ROS), physical contact with the cell membrane and indirect catalysis due to remnants from manufacture. The development and subsequent increasing usage of nanomaterials has highlighted a growing need to characterize and assess the toxicity of nanoparticles, particularly those that may have detrimental health effects such as carbon-based nanomaterials (CBNs). Due to interactions of nanoparticles with some reagents, many traditional toxicity tests are unsuitable for use with CBNs. Infrared (IR) spectroscopy is a non-destructive, high throughput technique, which is unhindered by such problems. We explored the application of IR spectroscopy to investigate the effects of CBNs on Gram-negative (*Pseudomonas fluorescens*) and Gram-positive (*Mycobacterium vanbaalenii* PYR-1) bacteria. Two types of IR spectroscopy were compared: attenuated total reflection Fourier-transform infrared (ATR-FTIR) and synchrotron radiation-based FTIR (SR-FTIR) spectroscopy. This showed that Gram-positive and Gram-negative bacteria exhibit differing alterations when exposed to CBNs. Gram-positive bacteria appear more resistant to these agents and this may be due to the protection afforded by their more sturdy cell wall. Markers of exposure also vary according to Gram status; Amide II was consistently altered in Gram-negative bacteria and carbohydrate altered in Gram-positive bacteria. ATR-FTIR and SR-FTIR spectroscopy could both be applied to extract biochemical alterations induced by each CBN that were consistent across the two bacterial species; these may represent potential biomarkers of nanoparticle-induced alterations. Vibrational spectroscopy approaches may provide a novel means of fingerprinting the effects of CBNs in target cells.

**Keywords:** Carbon-based nanoparticles; Gram-positive bacteria; Gram-negative bacteria; Nanotoxicity; Attenuated total reflection Fourier-transform infrared spectroscopy; Synchrotron radiation-based Fourier-transform infrared spectroscopy

## INTRODUCTION

Nanoparticles have unique physical, electrical and thermal properties, which make them useful in a wide range of applications in various industries including electronics and medicine.<sup>1</sup> A nanomaterial is defined as any material, whether natural or man-made, that has at least one external dimension <100 nm. Of the many materials associated with the nanotechnology revolution, carbon-based nanoparticles (CBNs) are thought to have some of the most diverse and distinct uses.<sup>2</sup> The first CBN, C<sub>60</sub>, also known as Buckminster fullerene was discovered in 1985. C<sub>60</sub> has carbon atoms laid out in a geodesic dome arrangement, giving it a spherical shape.<sup>3</sup> It was subsequently discovered that the process which yields fullerenes could also be used to generate multi-walled carbon nanotubes (MWCNTs); these are constructed of multiple layers of rolled, graphene sheets of varying diameters.<sup>4</sup> Manufacture of single-walled carbon nanotubes (SWCNT) was achieved in 1993. SWCNTs consist of a single tube, which looks similar to a rolled sheet of graphene; the carbon atoms form this structure by bonding in a hexagonal pattern.<sup>5</sup>

The growing usage of carbon-based nanomaterials has led to concern over their potential release into and effects on the environment. There are various routes by which nanomaterials can be released including liberation from nanocomposite polymers during their usage cycle, incineration, and during processing at wastewater treatment plants.<sup>6</sup> CBNs can exert toxic effects at the cellular level, primarily *via* generation of reactive oxygen species (ROS) and subsequent cellular oxidative stress.<sup>7</sup> Studies have shown that their ability to aggregate and physical contact of these particles with cell membranes plays a role in this toxicity.<sup>8, 9</sup> In addition, due to methods of manufacture, there are often metal impurities (remnants of catalysis) that can cause adverse effects.<sup>10</sup> CBNs have been shown to have deleterious effects on a range of organisms such as algae, protozoa, guinea pigs and humans.<sup>11-14</sup>

Bacteria have essential functions in many ecosystems. CBNs can be toxic to bacteria causing loss of viability in *Escherichia coli*<sup>8, 15, 16</sup> and in also more environmentally-relevant species such as *Bacillus subtilis* and *Pseudomonas aeruginosa*.<sup>17, 18</sup> A wide range of factors can affect the extent of toxicity such as size, surface area and purity of the nanoparticle,<sup>19</sup> cell membrane characteristics (whether the bacteria are Gram negative or positive),<sup>20</sup> and even the cell media used.<sup>21</sup> However, research into the effects of nanomaterials on bacteria has been hindered by the unsuitability of traditional cytotoxicity assays for use with nanoparticles. CBNs can interact with colorimetric reagent components of tests such as the MTT (3-[4,5-dimethylthiazol-2-yl]-2,5 diphenyl tetrazolium bromide), Neutral Red and other assays.<sup>22, 23</sup> CBNs commonly have large surface areas with hydrophobic properties, which are ideal for adsorption of dyes and many other molecules; this can invalidate the results of assays.<sup>24</sup> Such effects highlight the need to find better methods to assay nanoparticle effects and/or toxicity.

Infrared (IR) spectroscopy is a non-destructive, high throughput tool allowing analysis of biological samples. It exploits the principal that biochemical bonds can show some degree of movement such as stretching, bending, scissoring or twisting after absorption of energy from IR at specific wavelengths.<sup>25-27</sup> This absorbance is measured and generates spectra where peaks directly correlate to the structure of the material being investigated. The mid-IR region, known as the “biochemical-cell fingerprint” region, is where the majority of biochemical structures absorb IR energy and vibrate.<sup>28, 29</sup> This technique, coupled with multivariate analysis, allows identification of biochemical alterations induced by specific treatments.

Previously, we have used IR spectroscopy, specifically multi-beam synchrotron radiation-based Fourier-transform IR (SR-FTIR) spectroscopy, to investigate the effects of CBNs on Gram negative and positive bacteria.<sup>30</sup> Whilst the average, laboratory-based spectrometer uses a global IR source, SR sources produce much more brilliant light giving higher resolution due to the use of an accelerated electron beam.<sup>29</sup> This can be extremely

advantageous but synchrotron facilities are large, expensive and accessibility is often limited. The aim of the current paper was to use attenuated total reflection FTIR (ATR-FTIR) spectroscopy, which uses a global light source, with multivariate analysis to study the effects of CBNs on Gram-negative bacteria *Pseudomonas fluorescens* and Gram-positive bacteria *Mycobacterium vanbaalenii* PYR-1. Our specific aims were to explore CBN interactions with bacterial cells, as revealed by ATR-FTIR spectroscopy, and to compare these results with those generated by SR-FTIR spectroscopy.

## EXPERIMENTAL METHODS

### *Preparation of monocultures*

Gram-negative *P. fluorescens* and Gram-positive *M. vanbaalenii* PYR-1 were grown in an aqueous solution of mineral basal salts (MBS) with a phenanthrene growth substrate delivered using dimethylformamide (DMF) as a carrier solvent. Incubation of the cultures was undertaken in the dark at  $21 \pm 2^\circ\text{C}$ .

### *Experimental and control treatments*

Cell cultures were tested with one of four treatments: long multi-walled carbon nanotubes (MWCNTs; 110-170 nm diameter, 5-9  $\mu\text{m}$  length, >90% purity), short MWCNTs (10-15 nm diameter, 0.1-10  $\mu\text{m}$  length, >90% purity), fullerene soot and C<sub>60</sub> fullerene (1 nm, >99.5% purity, hereafter referred to as C60). All test agents were sourced from Sigma Aldrich Co. (Dorset, UK). We used  $10^7$  cells at the late exponential growth-phase of development (4 days for *P. flourescens* and 5 days for *M. vanbaalenii*) in each treatment; this standardisation being designed to avoid introduction of any bias associated with culture status, cell concentration or proportion of live / dead cells. Cells were harvested from liquid culture by centrifugation (3000 g for 5 min) and subsequent washing (three times) with sterile deionised water to remove growth media. Nanoparticles suspended in a 1% bovine serum

albumin (BSA - 98% purity; Sigma Aldrich Co.) and were diluted from a concentrated stock to deliver a concentration of  $0.01 \text{ mg}\cdot\text{L}^{-1}$  in 1 mL BSA to the live cell pellet. The BSA/nanoparticle mixture was vortex shaken for 1 min to disperse the cell pellet, then end-over-end shaken to prevent gravitational settling during a 2-h incubation period in the dark. Following incubation, bacterial cells were centrifuge-washed five times with 70% ethanol to thoroughly remove residual traces of BSA and fix the cells. The resulting cellular material was then applied to  $1 \text{ cm} \times 1 \text{ cm}$  Low-E reflective glass slides (Kevley Technologies, Chesterland, OH, USA), air-dried and stored in desiccators for at least 8 h prior to ATR-FTIR spectroscopy measurements.

Negative control samples of cells incubated with 1% BSA without CBNs were generated employing the same preparation protocol. Generation of ROS appears to be a major mechanism of nanotoxicity<sup>31</sup> and we generated positive control samples by exposing cells to ultraviolet (UV)-A radiation, a ROS-generating agent that is a suitable mediator of oxidative stress (OS) and outside the absorbance range of cellular components.<sup>32</sup>

Cultures for positive control experiments were grown, harvested and prepared for ATR-FTIR spectroscopy in exactly the same way as those tested with CBNs. Bacterial cells were re-suspended in 10 mL of 1% BSA and placed into T25 flasks. These positive control cultures were irradiated with UV-A delivered at a fluence rate of  $50 \text{ W}/\text{m}^2$  for 45 min (total dose =  $135 \text{ kJ}/\text{m}^2$ ) under four 36 Watt UV-A bulbs with emission peaks at 371 nm: conditions which have previously generated an ROS-stimulated response in bacteria.<sup>33</sup> Flasks were agitated after 20 min UV-A exposure to prevent the depletion of oxygen within the media and re-distribute bacteria. The temperature within T25 flasks was continuously monitored to ensure no excessive thermal accumulation was caused by UV-A treatment and that temperatures did not rise  $>27^\circ\text{C}$ . Non-UV-A irradiated positive control samples, wrapped in aluminium foil to block all light from reaching cells, were placed under UV-A lamps

alongside the UV-A irradiated samples to ensure an equivalence of conditions. All treatments and controls were conducted in triplicate.

#### *ATR-FTIR spectroscopy*

A Bruker TENSOR 27 FTIR spectrometer equipped with a Helios ATR diamond attachment (Bruker Optics Ltd, Coventry, UK) was used to acquire IR spectra. Spectra were acquired at  $4\text{ cm}^{-1}$  resolution, 2.2 kHz mirror velocity and 32 co-additions. A total of 10 spectra were acquired per slide, specifically from areas containing agglomerates of CBNs visible through the ATR magnification-limited viewfinder camera. The crystal was cleaned with deionised water and background readings re-taken prior to measurement of each new sample. Spectra acquired from nanoparticles alone did not show any peaks in the biochemical-cell fingerprint range ( $1800\text{ cm}^{-1}$  -  $900\text{ cm}^{-1}$ ); hence, acquired spectra reveal the effects of CBNs rather than the nanoparticles themselves.

#### *Pre-processing of spectra and PCA-LDA*

All data processing was carried out using MATLAB r2012b (The MathWorks Inc., US) with our in-house toolbox (<http://bioph.lancs.ac.uk/iroot>). Each of the acquired IR spectra was cut to the biochemical-cell fingerprint region ( $1800\text{ cm}^{-1}$  -  $900\text{ cm}^{-1}$ ), baseline corrected by 1<sup>st</sup> order differentiation and then vector normalised. Spectra were acquired at  $3.84\text{ cm}^{-1}$  resolution giving rise to 235 absorbance intensities per IR spectrum. The optimum number of PC factors for subsequent input into LDA was calculated for each dataset separately through an optimization procedure using classification [see Supplementary Information (SI) Figure S1 and Table S1]. Cross-calculated principal component analysis (PCA)-linear discriminant analysis (LDA) was then applied to each dataset where appropriate. The leave-one-out cross-validation method uses a small portion of the dataset to train the model in order to prevent LDA overfitting. LDA applied to each of the selected PCs maximizes inter-class variance relative to intra-class variance, allowing maximum separation

of PCA-LDA scores between CBN treatments, and subsequently allows the wavenumbers responsible for the separation of the scores to be determined.<sup>28, 34</sup>

#### *PCA-LDA cluster vector*

To highlight important biomarkers related to each class of data, the cluster vectors approach is employed. Simplification of agent-induced biochemical alterations relative to the corresponding vehicle control is achieved by moving the centre of the control cluster itself to the origin of the PCA-LDA factor space, hence making the control cluster vector, which represents no biochemical alteration, the zero vector.<sup>35</sup> The extent of peak deviation away from the origin of the factor space then occurs proportional to the extent of biochemical alteration according to the centre of each corresponding agent-induced cluster.

#### *Statistical analysis*

For the purposes of statistical analysis, the spectra from each treatment class were pooled and each IR spectrum was treated as a replicate, as previously described.<sup>36</sup> One-way analysis of variance (ANOVA) with Tukey's post hoc test was employed to test the differences in scores between all CBN treatment classes. Unpaired two-tailed *t*-tests were used to test the differences between scores from UV-A irradiated and non-UV-A irradiated positive control samples. All statistical analysis was carried out in GraphPad Prism 4.

## **RESULTS AND DISCUSSION**

#### *Effects of CBNs on bacteria*

A scores plot for *P. fluorescens* (Fig. 1) shows distinct clustering for all treatment categories away from the control cluster of spectral points with the most profound being associated with cells treated with C<sub>60</sub>. The clusters for short or long MWCNTs, fullerene soot and the control are all relatively close to each other along LD1 and LD2 whereas, for C<sub>60</sub>, there is very clear separation along LD1 and LD3. C<sub>60</sub> induces segregation that is much

further away from the control category compared to other CBN treatments and a one-way ANOVA with Tukey's post-hoc test (Table 1A) indicates that although all CBNs are significantly different from each other along LD1, C<sub>60</sub> is the only treatment to differ significantly from the control category along this axis. The *M. vanbaalenii* PCA-LDA scores plot (Fig. 2) indicates that CBN treatments resulted in obvious cluster segregation. Long MWCNTs and C<sub>60</sub> treatment resulted in the most separation and distance away from the corresponding control but all CBN-treated cell clusters are to some extent segregated. All treatment categories are significantly different from the control category along LDs 1, 2 and 3 except for short MWCNTs on LD2 (Table 1B). All treatment categories also differ from each other except long and short MWCNTs on LD1. Short MWCNTs and fullerene soot are the closest to the control category suggesting that these two treatments induce the least marked bacterial-cell alterations.

Cluster vectors plots separate categories from the corresponding control spectral cluster based on wavenumber, thus allowing identification of biomarkers of exposure to CBNs. The five largest peaks for *P. fluorescens* were picked from cluster vectors plots using a peak detection algorithm (Fig. 3) and tentative wavenumber alterations assigned (Table 2). Short MWCNTs (Table 2A) induced the most marked alterations in DNA, protein (Amide I and II) and lipid regions whereas long MWCNTs (Table 2B) caused alterations to symmetric phosphate stretching vibrations ( $\nu_s\text{PO}_2^-$ ), lipid, carbohydrate and protein (Amide II). Fullerene soot exposure (Table 2D) also generated a similar profile of alterations, associated with asymmetric phosphate stretching vibrations ( $\nu_{as}\text{PO}_2^-$ ) and  $\nu_s\text{PO}_2^-$ , DNA, protein (Amide II) and lipid. C<sub>60</sub> (Table 2C) induced more extensive protein alterations. The top four peak assignments are in the protein region with the fifth associated with alterations to carbohydrates. Thus, short MWCNTs, long MWCNTs and fullerene soot induce fairly similar patterns of spectral alterations whereas C<sub>60</sub> is distinctly different. This reflects the extent of

dissimilarity in the PCA-LDA scores plot (Fig. 1) and may be due to a relationship between size and toxicity, as toxic effects of nanoparticles are related to particle size due to an increase in surface area to volume ratio.<sup>8,37</sup> C<sub>60</sub> is the smallest CBN tested and it also caused the most distinct and extensive alterations whereas long MWCNTs (the largest CBN) induced the least marked alterations.

A cluster vectors peak detection plot (Fig. 4) and tentative peak assignments (Table 3) shows that in *M. vanbaalenii*, short MWCNTs (Table 3A) cause extensive alterations in carbohydrate, proteins and DNA. Long MWCNTs (Table 3B) induce protein (Amide II), carbohydrate and DNA alterations with C<sub>60</sub> (Table 3C) inducing changes in polysaccharides, other carbohydrates and  $\nu_{\text{as}}\text{PO}_2^-$ . Fullerene soot (Table 3D) also affects carbohydrates including polysaccharides as well as lipid and protein (Amide II). Both short and long MWCNTs induce similar alterations in these bacteria and fullerene soot shares some of these characteristics. However, as with *P. fluorescens*, C<sub>60</sub> had a different spectral profile in *M. vanbaalenii* as alterations are more associated with carbohydrate alterations.

#### *Differences between Gram-negative and Gram-positive bacteria*

There are many factors that can affect the toxicity that nanoparticles exert on bacteria, one of which is the species of bacteria and their associated membrane characteristics.<sup>38</sup> Gram-negative and Gram-positive bacteria have been shown to exhibit different responses to nanoparticles.<sup>17</sup> Gram-positive *M. vanbaalenii* display a much greater separation between treatment category clusters and from the control (Fig. 2) than that seen in Gram-negative *P. fluorescens*, which exhibits more overlap (Fig. 1). This overlap of CBN-treatment categories suggests that these bacteria are fairly equally affected (or unaffected) by the nanoparticles. The enhanced separation seen in *M. vanbaalenii* category clusters could indicate that it is affected differently by the various CBN types and to differing extents. Gram-positive bacteria such as *M. vanbaalenii* have a thick ring of peptidoglycan and teichoic acid around their cell

wall which increases structural integrity<sup>39</sup> and may be protective, thereby increasing robustness against some types of CBN.<sup>17</sup> The peptidoglycan layer in Gram-negative bacteria is thinner and also overlaid by a membrane layer meaning that these bacteria may be unable to withstand nanotoxic assault in the same way.

Despite differences in membrane structures and the potential variation this can cause, C<sub>60</sub> (Table 2C and 3C) caused the most extensive and marked alterations in both bacteria, perhaps due to its small size and relatively large surface area. However, the alterations induced in each species were not the same. In *P. fluorescens*, the alterations were mainly in proteins particularly Amide I and II (Fig. 3) but in *M. vanbaalenii*, there were more carbohydrate changes (Table 3C). C<sub>60</sub> has been found to cause toxic effects by direct contact with cells<sup>40</sup> and as peptidoglycan has a carbohydrate backbone, this may explain why carbohydrate changes were so predominant in the Gram-positive bacteria. In *P. fluorescens* treated with long or short MWCNTs or fullerene soot, lipid alterations were in the top five peaks detected whereas these were not present in any of the top peak assignments for *M. vanbaalenii*. Gram-negative bacteria have a membrane layer on their outermost surface of the cell so increased lipid alterations could be expected without a strong peptidoglycan layer for protection. In *P. fluorescens*, the only biomolecule that was consistently affected by CBNs was Amide II and in *M. vanbaalenii*, carbohydrates were altered. These biomarker effects may represent key biochemical changes, which signature nanotoxicity in these different bacterial species.

#### *Positive controls*

There are many hypotheses regarding the exact mechanisms of toxicity employed by carbon nanoparticles, one of which is that nanotoxicity is caused by the generation of ROS.<sup>7</sup> With this in mind, UV-A was used as a positive control for ROS generation. In both *P. fluorescens* (Fig. 5A) and *M. vanbaalenii* (Fig. 5B), UV-A irradiation induced alterations in

lipids and proteins (Amide I) (Fig. 5; Table 4), which are consistent with ROS-induced damage such as lipid peroxidation. Two-tailed, unpaired *t*-tests (Table 4) show that UV-A treated bacterial cells are significantly different from the non-UV-A exposed corresponding negative controls.

As UV-A is considered to be an independent oxidative stress-inducing mechanism; employing this treatment as a positive control allowed us to assess whether any of the CBNs tested generate ROS. In *P. fluorescens*, some of the CBNs did induce alterations in lipid and Amide I in the top five alterations, although not to the same extent as observed in UV-A-treated cells. Fullerene soot and long MWCNTs induced lipid alterations and C<sub>60</sub> caused extensive Amide I alterations. However, exposure with short MWCNTs generated the most ROS-like spectral profile, causing significant alterations in both Amide I and lipid. Alterations induced by CBNs in *M. vanbaalenii* were less like those caused by UV-A. Only fullerene soot generated lipid alterations to such an extent that it appears in the top five peaks in cluster vectors plots and no CBN caused Amide I changes. These results suggest that although ROS generation may not appear to be the primary mechanism of nanotoxicity, it may have a role to play particularly in *P. fluorescens* treated with short MWCNTs. Other studies have shown that Gram-negative bacteria are more susceptible to nanoparticles than Gram-positive bacteria due to the lipopolysaccharide in the membrane facilitating better interaction between the cell and nanoparticle.<sup>41, 42</sup> More ROS-like activity may be seen in *P. fluorescens* than in *M. vanbaalenii* as its Gram-negative status allows CBNs to cluster onto the surface of the cells and generate the molecules that cause oxidative stress.

#### *Comparison to SR-FTIR spectroscopy*

Our previous work in this area has utilised SR-FTIR spectroscopy to analyse the effect of CBNs on bacteria and other cells.<sup>30</sup> By comparing our results from this present study with those collected using the exact same experimental procedures but analysed by SR-FTIR

spectroscopy (see SI, Tables S2 - S4), we can assess how comparable both techniques are towards detecting CBN-induced changes in bacteria.<sup>43, 44</sup> Pre-processing methods for both datasets were kept as similar as possible, providing they were appropriate, in order to prevent unnecessary variance. Both SR-FTIR and ATR-FTIR spectroscopy picked out the major trends in cluster separation in both bacterial species. They both showed that *M. vanbaalenii* exhibited better clustering and separation of category clusters whereas *P. fluorescens* had less defined clusters with much more overlap between categories. C<sub>60</sub> was consistently detected as the CBN whose exposure resulted in spectral clusters that are furthest away from the control, with the most extensive alterations. The category cluster distance from the corresponding control in both bacterial species followed the order of C<sub>60</sub> (the furthest), then MWCNTs and then fullerene soot; this was observed in both SR-FTIR and ATR-FTIR spectrochemical data.

In terms of biochemical alterations, data for *P. fluorescens* (see SI, Tables S2 and S3) from both spectroscopy techniques was fairly comparable. The top five peaks from each spectrochemical dataset did not match to exact wavenumbers and magnitude order but the overall trends in alterations were the same. With both techniques, short MWCNTs caused changes in DNA, protein and lipid, long MWCNTs altered protein and DNA, and fullerene soot caused alterations in protein, carbohydrate and lipid regions. C<sub>60</sub> is a good example of where both techniques showed an alteration in the same top five peaks in cluster vectors plots but the magnitude of individual ones differed. Both techniques showed carbohydrate as being one of the most extensively altered biomolecules but SR-FTIR spectroscopy showed it to be the most altered whereas ATR-FTIR spectroscopy ranked it as fifth. Alterations caused by CBNs in *M. vanbaalenii* (Table 3) did not compare across both techniques as the top peaks were very different. This may have been because it is a Gram-positive bacterium and as the peptidoglycan could offer protection against nanotoxicity, we saw a greater range of alteration caused by the CBNs. In Gram-negative bacteria, CBNs come up against minimal

buffers to their toxic assault and so all cause a similar extent of alteration. This coupled with instrumental and sample differences could have influenced the consistency of biochemical alterations across the two techniques. A major difference would be the spatial resolution of both methods employed with that of SR-FTIR spectroscopy being much greater compared to that of ATR-FTIR spectroscopy; this could explain why the former technique isolated carbohydrate alterations as being major because it could focus better on cell membranes.

ATR-FTIR and SR-FTIR spectroscopy were could both be applied to extract biochemical alterations induced by each CBN that were constant across the two bacterial species; these may represent potential biomarkers. Both techniques detected the same biomarkers but SR-FTIR seemed able to identify more. For example, for short MWCNTs, ATR-FTIR spectroscopy (Tables S3 and S5) showed Amide I as a consistent biomarker which SR-FTIR spectroscopy was able to detect (see SI, Table S2 and S4) but it also showed that lipid and DNA were reproducibly altered. SR-FTIR spectroscopy detected more biomarkers than ATR-FTIR spectroscopy following exposure to all CBNs except in fullerene soot where the biomarkers (alterations in Amide II, lipids and carbohydrates) were exactly the same when extracted by either technique. There were also some areas where the two spectroscopic techniques were not comparable at all. SR-FTIR data showed that Amide I was altered following exposure to all CBNs tested irrespective of bacterial-cell types, which indicates that this might be an overall marker of nanotoxicity. It also detected that lipid alterations were significant. This was less apparent using ATR-FTIR spectroscopy.

ATR-FTIR and SR-FTIR spectroscopy did appear to generate comparable data but there are limitations to how interchangeable the two techniques are. Generally, ATR-FTIR spectroscopy did reveal the same information as SR-FTIR spectroscopy but in less detail; it seemed to analyse the overall trends in alterations in comparison to the detail that was

revealed by SR-FTIR spectroscopy. However, given that the value of SR-FTIR spectroscopy is its superior resolution, it was not surprising that more could be elucidated about the dataset.

## CONCLUSIONS

IR spectroscopy with multivariate analysis is a robust tool for the investigation of CBN-cell interactions.<sup>45</sup> This study has shown that CBNs induced a profile of alterations in Gram-negative and Gram-positive bacteria. Gram-positive bacteria exhibit more variance in the extent of these alterations, possibly due to the protective effect of their thick peptidoglycan layer, which potentially gives these cells greater structural integrity against CBN-mediated damage such as ROS generation. Potential biomarkers of exposure to CBNs also varied with membrane characteristics; in Gram-negative *P. fluorescens*, Amide II alterations were seen consistently across all nanoparticle types and in Gram-positive *M. vanbaalenii*, carbohydrate was the potential marker. In both bacteria, the nanoparticles induced a similar ranking of alteration extent with C<sub>60</sub> causing the most significant differences. We also compared ATR-FTIR and SR-FTIR spectroscopy and found that, although there were some differences between the two methods, overall, the information retrieved was largely comparable. SR-FTIR spectroscopy provided detailed, in-depth information on nanotoxic alterations due to its superior resolution whereas ATR-FTIR spectroscopy was less exhaustive, pulling out fewer biomarkers, but it provided an excellent overview and reasonable detail of alterations induced by CBNs.

**Acknowledgments:** Kelly Heys is a NERC-CEH algorithm student.

## REFERENCES

1. C.W. Lam, J.T. James, R. McCluskey, S. Arepalli and R.L. Hunter, A review of carbon nanotube toxicity and assessment of potential occupational and environmental health risks. *Crit. Rev. Toxicol.*, 2006, **36(3)**, 189-217.
2. H.J. Johnston, G.R. Hutchison, F.M. Christensen, S. Peters, S. Hankin, K. Aschberger and V. Stone, A critical review of the biological mechanisms underlying the *in vivo* and *in vitro* toxicity of carbon nanotubes: The contribution of physico-chemical characteristics. *Nanotoxicology*, 2010, **4(2)**, 207-246.
3. Kroto, K.W., J.R. Heath, S.C. O'Brien, R.F. Curl and S.R. E., C<sub>60</sub>: Buckminsterfullerene. *Nature*, 1985, **318**, 162-163.
4. Iijima, S., Helical microtubules of graphitic carbon. *Nature*, 1991, **354**, 56-58.
5. Iijima, S. and T. Ichihashi, Single-shell carbon nanotubes of 1-nm diameter. *Nature*, 1993, **363**, 603-605.
6. E.J. Petersen, L. Zhang, N.T. Mattison, D.M. O'Carroll, A.J. Whelton, N. Uddin, T. Nguyen, Q.G. Huang, T.B. Henry, R.D. Holbrook and K.L. Chen, Potential release pathways, environmental fate, and ecological risks of carbon nanotubes. *Env. Sci. Technol.*, 2011, **45(23)**, 9837-9856.
7. A.A. Shvedova, A. Pietroiusti, B. Fadeel and V.E. Kagan, Mechanisms of carbon nanotube-induced toxicity: Focus on oxidative stress. *Toxicol. Appl. Pharmacol.*, 2012, **261(2)**, 121-133.
8. S. Kang, M. Pinault, L.D. Pfefferle and M. Elimelech, Single-walled carbon nanotubes exhibit strong antimicrobial activity. *Langmuir*, 2007, **23(17)**, 8670-8673.
9. S.B. Lee, R. Koepsel, D.B. Stolz, H.E. Warriner and A.J. Russell, Self-assembly of biocidal nanotubes from a single-chain diacetylene amine salt. *J. Am. Chem. Soc.*, 2004, **126(41)**, 13400-13405.
10. K. Pulskamp, J.M. Wörle-Knirsch, F. Henrich, K. Kern and H.F. Krug, Human lung epithelial cells show biphasic oxidative burst after single-walled carbon nanotube contact. *Carbon*, 2007, **45(11)**, 2241-2249.
11. E.J. Petersen, J. Akkanen, J.V.K. Kukkonen and W.J. Weber, Biological uptake and depuration of carbon nano-tubes by *Daphnia magna*. *Environ. Sci. Technol.*, 2009, **43(8)**, 2969-2975.
12. P. Ghafari, C.H. St-Denis, M.E. Power, X. Jin, V. Tsou, H.S. Mandal, N.C. Bols and X.W. Tang, Impact of carbon nanotubes on the ingestion and digestion of bacteria by ciliated protozoa. *Nature Nanotechnol.*, 2008, **3**, 347-351.
13. A. Huczko, H. Lange, M. Bystrzejewski, P. Baranowski, H. Grubek-Jaworska, P. Nejman, T. Przybyłowski, K. Czumińska, J. Glapiński, D.R.M. Walton and H.W. Kroto, Pulmonary toxicity of 1-D nanocarbon materials. *Fuller. Nanotub. Car. N.*, 2005, **13(2)**, 141-145.

14. N.A. Monteiro-Riviere, R.J. Nemanich, A.O. Inman, Y.Y.Y. Wang and J.E. Riviere, Multi-walled carbon nanotube interactions with human epidermal keratinocytes. *Toxicol. Lett.*, 2005, **155(3)**, 377-384.
15. A. Simon-Deckers, S. Loo, M. Mayne-L'Hermite, N. Herlin-Boime, N. Menguy, C. Reynaud, B. Gouget and M. Carriere, Size-, composition- and shape-dependent toxicological impact of metal oxide nanoparticles and carbon nanotubes toward bacteria. *Env. Sci. Technol.*, 2009, **43(21)**, 8423-8429.
16. D.F. Rodrigues and M. Elimelech, Toxic effects of single-walled carbon nanotubes in the development of *E. coli* biofilm. *Env. Sci. Technol.*, 2010, **44(12)**, 4583-4589.
17. S. Kang, M.S. Mauter and M. Elimelech, Microbial cytotoxicity of carbon-based nanomaterials: implications for river water and wastewater effluent. *Env. Sci. Technol.*, 2009, **43(7)**, 2648-2653.
18. S. Liu, L. Wei, L. Hao, N. Fang, M.W. Chang, R. Xu, Y. Yang and Y. Chen, Sharper and faster "nano darts" kill more bacteria: a study of antibacterial activity of individually dispersed pristine single-walled carbon nanotube. *ACS Nano*, 2009, **3(12)**, 3891-3902.
19. G. Jia, H Wang, L. Yan, X. Wang, R Pei, T. Yan, Y. Zhao and X. Guo, Cytotoxicity of carbon nanomaterials: Single-wall nanotube, multi-wall nanotube, and fullerene. *Environ. Sci. Technol.*, 2005, **39(5)**, 1378-1383.
20. J. Fang, D.Y. Lyon, M.R. Wiesner, J.P. Dong and P.J.J. Alvarez, Effect of a fullerene water suspension on bacterial phospholipids and membrane phase behavior. *Environ. Sci. Technol.*, 2007, **41(7)**, 2636-2642.
21. Y. Zhu, T. Ran, Y. Li, J. Guo and W. Li, Dependence of the cytotoxicity of multi-walled carbon nanotubes on the culture medium. *Nanotechnology*, 2006, **17(18)**, 4668-4674.
22. J.M. Worle-Knirsch, K. Pulskamp and H.F. Krug, Oops they did it again! Carbon nanotubes hoax scientists in viability assays. *Nano Lett.*, 2006, **6(6)**, 1261-1268.
23. A. Casey, E. Herzog, M. Davoren, F.M. Lyng, H.J. Byrne and G. Chambers, Spectroscopic analysis confirms the interactions between single walled carbon nanotubes and various dyes commonly used to assess cytotoxicity. *Carbon*, 2007, **45(7)**, 1425-1432.
24. R.H. Hurt, M. Monthieux and A. Kane, Toxicology of carbon nanomaterials: Status, trends, and perspectives on the special issue. *Carbon*, 2006, **44(6)**, 1028-1033.
25. M. Picquart, E. Haro-Poniatowski, J.F. Morhange, M. Jouanne and M. Kanehisa, Low frequency vibrations and structural characterization of a murine IgG2a monoclonal antibody studied by Raman and IR spectroscopies. *Biopolymers*, 2000, **53(4)**, 342-349.
26. M.W. Nydegger, W. Rock and C.M. Cheatum, 2D IR Spectroscopy of the C-D stretching vibration of the deuterated formic acid dimer. *Phys. Chem. Chem. Phys.*, 2011, **13(13)**, 6098-6104.

27. E. Podstawka-Proniewicz, N. Piergies, D. Skoluba, P. Kafarski, Y. Kim and L.M. Proniewicz, Vibrational characterization of L-leucine phosphonate analogues: FT-IR, FT-Raman, and SERS spectroscopy studies and DFT Calculations. *J. Phys. Chem. A*, 2011, **115(40)**, 11067-11078.
28. F.L. Martin, J.G. Kelly, V. Llabjani, P.L. Martin-Hirsch, Patel, II, J. Trevisan, N.J. Fullwood and M.J. Walsh, Distinguishing cell types or populations based on the computational analysis of their infrared spectra. *Nat. Protoc.*, 2010, **5(11)**, 1748-1760.
29. J.G. Kelly, J. Trevisan, A.D. Scott, P.L. Carmichael, H.M. Pollock, P.L. Martin-Hirsch and F.L. Martin, Biospectroscopy to metabolically profile biomolecular structure: a multistage approach linking computational analysis with biomarkers. *J. Proteome Res.*, 2011, **10**, 1437-1448.
30. M.J. Riding, J. Trevisan, C.J. Hirschmugl, K.C. Jones, K.T. Semple and F.L. Martin, Mechanistic insights into nanotoxicity determined by synchrotron radiation-based Fourier-transform infrared imaging and multivariate analysis. *Environ. Int.*, 2012, **50**, 56-65.
31. Wani, M.Y., M.A. Hashim, F. Nabi and M.A. Malik, Nanotoxicity: dimensional and morphological concerns. *Adv. Phys. Chem.*, 2011, 450912.
32. R.L. Wells and A. Han, Action spectra for killing and mutation of Chinese hamster cells exposed to mid- and near-ultraviolet monochromatic light. *Mutat. Res.*, 1984, **129(2)**, 251-258.
33. J.D. Hoerter, A.A. Arnold, D.A. Kuczynska, A. Shibuya, C.S. Ward, M.G. Sauer, A. Gizachew, T.M. Hotchkiss, T.J. Fleming and S. Johnson, Effects of sublethal UVA irradiation on activity levels of oxidative defense enzymes and protein oxidation in *Escherichia coli*. *J. Photochem. Photobiol. B*, 2005, **81(3)**, 171-180.
34. F.L. Martin, M.J. German, E. Wit, T. Fearn, N. Ragavan and H.M. Pollock, Identifying variables responsible for clustering in discriminant analysis of data from infrared microspectroscopy of a biological sample. *J. Comput. Biol.*, 2007, **14(9)**, 1176-1184.
35. V. Llabjani, J. Trevisan, K.C. Jones, R.F. Shore and F.L. Martin, Binary mixture effects by PBDE congeners (47, 153, 183, or 209) and PCB congeners (126 or 153) in MCF-7 cells: Biochemical alterations assessed by IR spectroscopy and multivariate analysis. *Environ. Sci. Technol.*, 2010, **44(10)**, 3992-3998.
36. V. Llabjani, J. Trevisan, K.C. Jones, R.F. Shore and F.L. Martin, Derivation by infrared spectroscopy with multivariate analysis of bimodal contaminant-induced dose-response effects in MCF-7 cells. *Environ. Sci. Technol.*, 2011, **45(14)**, 6129-6135.
37. L. Nyberg, R.F. Turco and L. Nies, Assessing the impact of nanomaterials on anaerobic microbial communities. *Environ. Sci. Technol.*, 2008, **42(6)**, 1938-1943.
38. D.M. Aruguete and M.F. Hochella, Bacteria-nanoparticle interactions and their environmental implications. *Environ. Chem.*, 2010, **7(1)**, 3-9.

39. J.R. Scott and T.C. Barnett, Surface proteins of gram-positive bacteria and how they get there. *Annu. Rev. Microbiol.*, 2006, **60**, 397-423.
40. D.Y. Lyon and P.J. Alvarez, Fullerene water suspension (nC60) exerts antibacterial effects via ROS-independent protein oxidation. *Environ. Sci. Technol.*, 2008, **42(21)**, 8127-8132.
41. S. Shrivastava, T. Bera, A. Roy, G. Singh, P. Ramachandrarao and D. Dash, Characterization of enhanced antibacterial effects of novel silver nanoparticles. *Nanotechnology*, 2007, **18(22)**, 225103.
42. M.J. Riding, F. L. Martin, J. Trevisan, V. Llabjani, I.I. Patel, K.C. Jones KC and K.T. Semple, Concentration-dependent effects of carbon nanoparticles in gram-negative bacteria determined by infrared spectroscopy with multivariate analysis. *Environ. Pollut.*, 2012, **163**, 226-234.
43. J. Trevisan, P.P. Angelov, A.D. Scott, P.L. Carmichael and F.L. Martin, IRootLab: a free and open-source MATLAB toolbox for vibrational biospectroscopy data analysis. *Bioinformatics*, 2013, **29(8)**, 1095-1097.
44. J. Trevisan, P.P. Angelov, P.L. Carmichael, A.D. Scott and F.L. Martin, Extracting biological information with computational analysis of Fourier-transform infrared (FTIR) biospectroscopy datasets: current practices to future perspectives. *Analyst*, 2012, 137(14), 3202-3215.
45. J. Li, R. Strong, J. Trevisan, S.W. Fogarty, N.J. Fullwood, K.C. Jones and F.L. Martin, Dose-related alterations of carbon nanoparticles in mammalian cells using biospectroscopy: potential for real-world effects. *Environ. Sci. Technol.*, **47(17)**, 10005-10011.

## Legends to Figures

**Figure 1** Three-dimensional (3-D) scatter plot, derived from cross-validated principal component analysis-linear discriminant analysis (PCA-LDA), for *P. fluorescens* treated with 0.01 mg.L<sup>-1</sup> of carbon-based nanoparticles (CBNs). Infrared (IR) spectra are reduced to single points with PCA-LDA and subsequently plotted in 3-D. For clarity, 95% confidence intervals have been plotted on each axis.

**Figure 2** Three-dimensional (3-D) scatter plot, derived from cross-validated principal component analysis-linear discriminant analysis (PCA-LDA), for *M. vanbaalenii* treated with 0.01 mg.L<sup>-1</sup> of carbon-based nanoparticles (CBNs). Infrared (IR) spectra are reduced to single points with PCA-LDA and are plotted in 3-D. For clarity, 95% confidence intervals have been plotted on each axis.

**Figure 3** One-dimensional, peak detection cluster vector plot, for *P. fluorescens* treated with 0.01 mg.L<sup>-1</sup> of CBNs.

**Figure 4** One-dimensional, peak detection cluster vectors plot, for *M. vanbaalenii* treated with 0.01 mg.L<sup>-1</sup> of CBNs.

**Figure 5** Cross-validated principal component analysis-linear discriminant analysis (PCA-LDA) loadings plots of positive control samples for (A) *P. fluorescens*; and, (B) *M. vanbaalenii* irradiated with ultraviolet (UV)-A for 45 minutes.

Figure 1

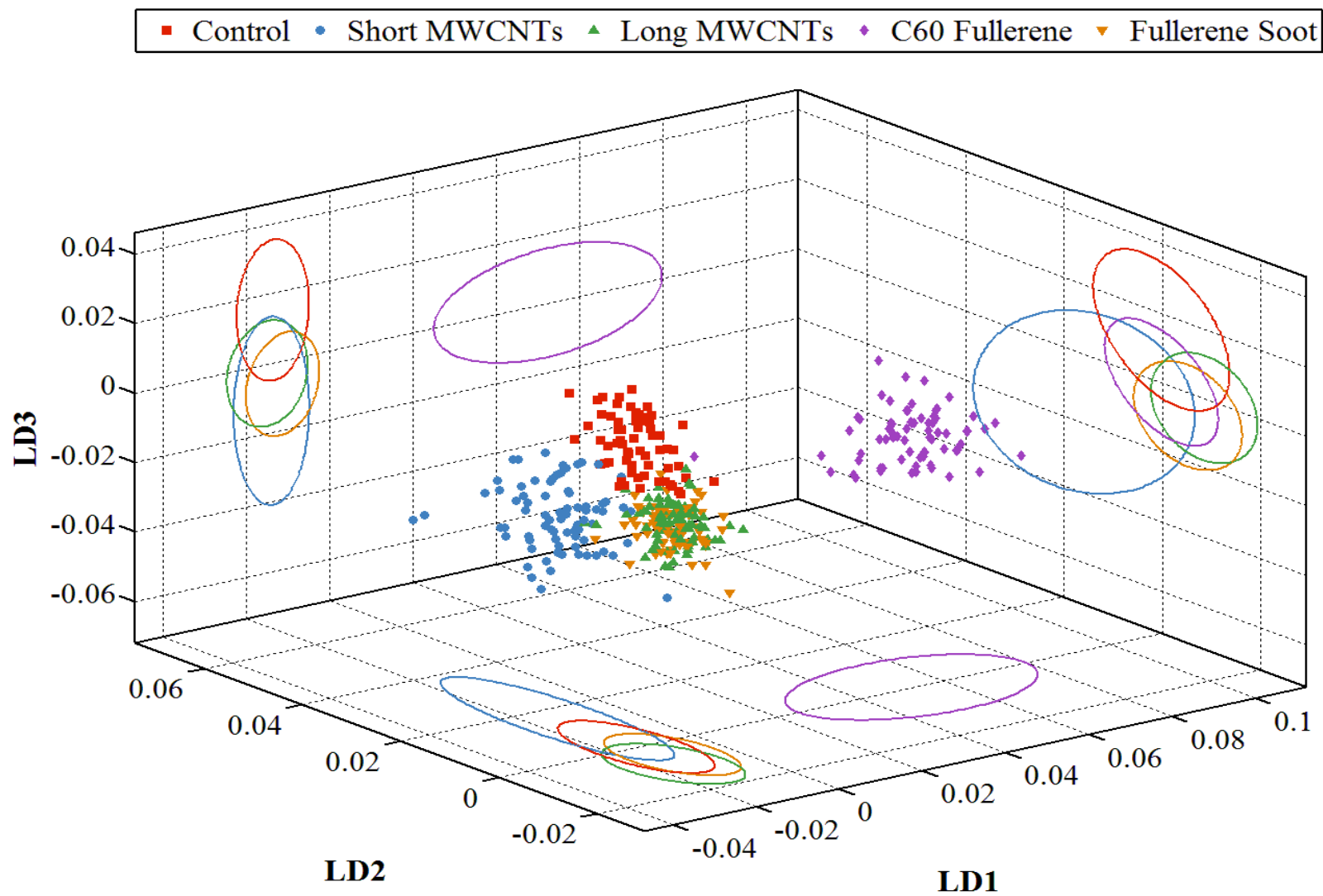


Figure 2

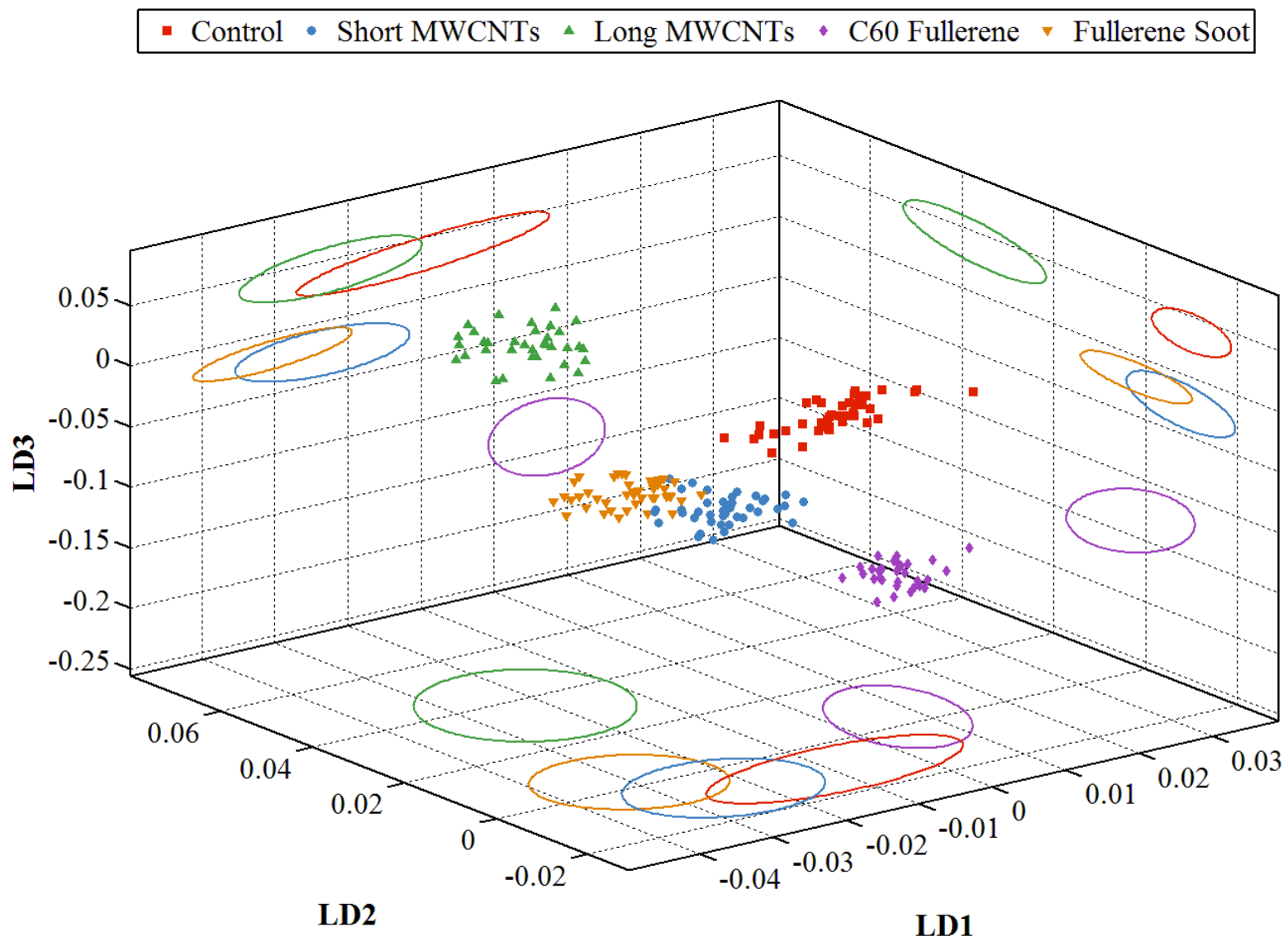


Figure 3

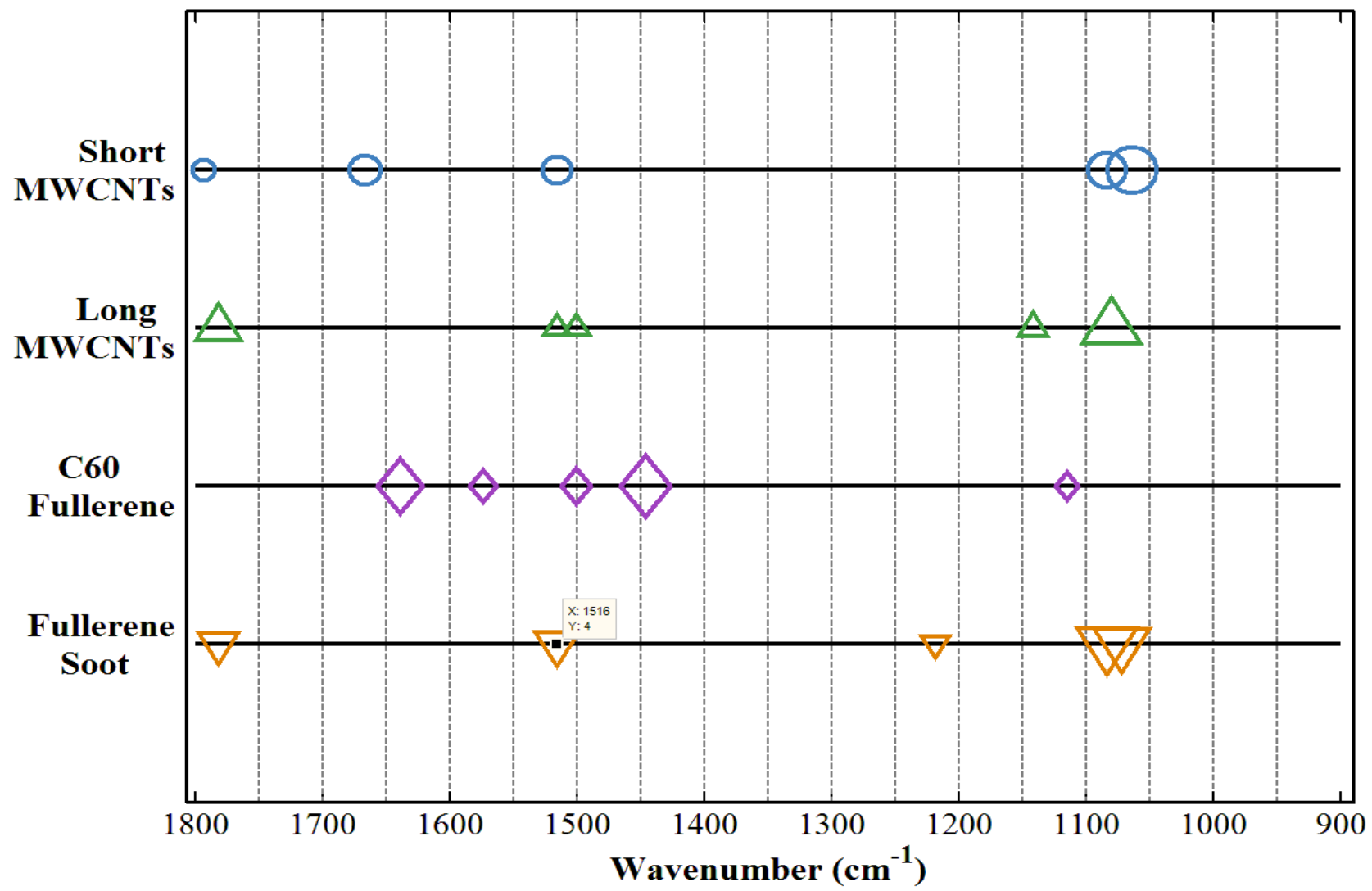


Figure 4

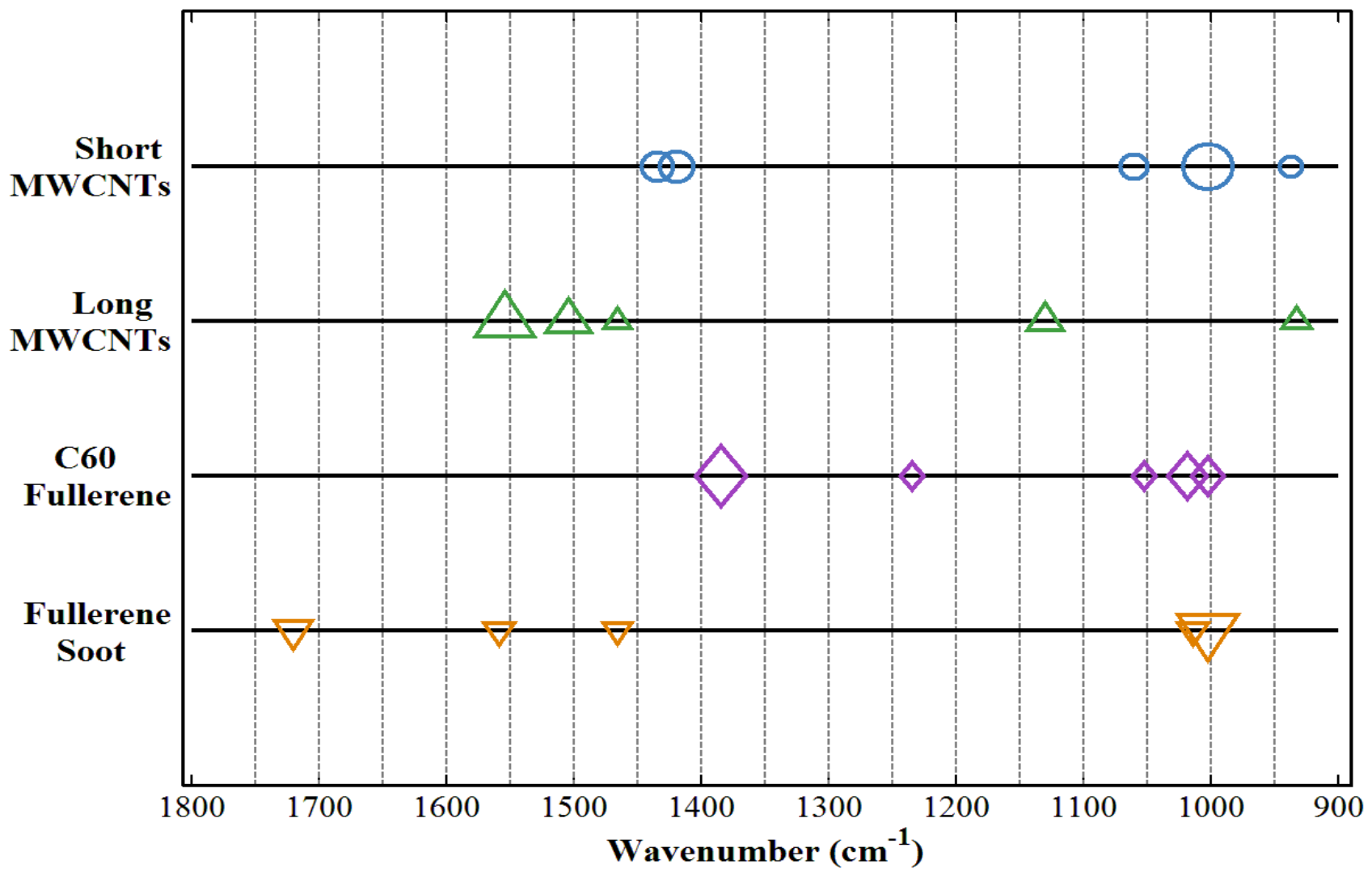
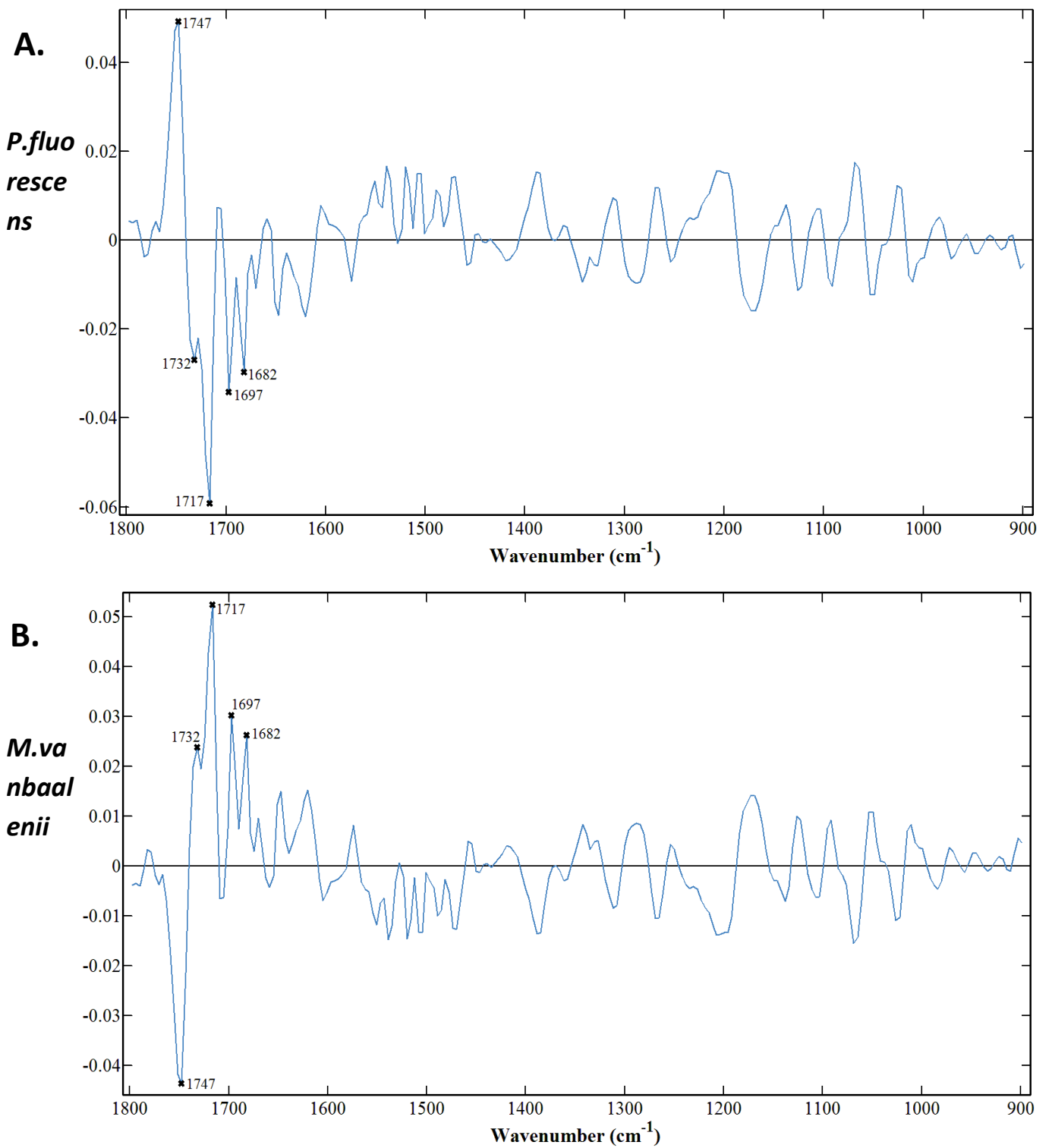


Figure 5



**Table 1.** *P*-values, calculated by one-way ANOVA with Tukey's post-hoc test, for (A) *P. fluorescens* and (B) *M. vanbaalenii* treated with 0.01 mg.L<sup>-1</sup> of CBNs. Red indicates results that are not significant.

**A.**

Treatment comparisons	LD1	LD2	LD3
Control vs. Short MWCNTs	<i>P</i> > 0.05	<i>P</i> < 0.001	<i>P</i> < 0.001
Control vs. Long MWCNTs	<i>P</i> > 0.05	<i>P</i> < 0.001	<i>P</i> < 0.001
Control vs. C60 Fullerene	<i>P</i> < 0.001	<i>P</i> > 0.05	<i>P</i> < 0.001
Control vs. Fullerene Soot	<i>P</i> > 0.05	<i>P</i> < 0.001	<i>P</i> < 0.001
Short MWCNTs vs. Long MWCNTs	<i>P</i> > 0.05	<i>P</i> < 0.001	<i>P</i> < 0.001
Short MWCNTs vs. C60 Fullerene	<i>P</i> < 0.001	<i>P</i> < 0.001	<i>P</i> < 0.001
Short MWCNTs vs. Fullerene Soot	<i>P</i> < 0.05	<i>P</i> < 0.001	<i>P</i> < 0.001
Long MWCNTs vs. C60 Fullerene	<i>P</i> < 0.001	<i>P</i> < 0.001	<i>P</i> > 0.05
Long MWCNTs vs. Fullerene Soot	<i>P</i> < 0.001	<i>P</i> < 0.01	<i>P</i> < 0.01
C60 Fullerene vs. Fullerene Soot	<i>P</i> < 0.001	<i>P</i> < 0.001	<i>P</i> < 0.001

**B.**

Treatment comparisons	LD1	LD2	LD3
Control vs. Short MWCNTs	<i>P</i> < 0.001	<i>P</i> > 0.05	<i>P</i> < 0.001
Control vs. Long MWCNTs	<i>P</i> < 0.001	<i>P</i> < 0.001	<i>P</i> < 0.05
Control vs. C60 Fullerene	<i>P</i> < 0.001	<i>P</i> < 0.001	<i>P</i> < 0.001
Control vs. Fullerene Soot	<i>P</i> < 0.001	<i>P</i> < 0.001	<i>P</i> < 0.001
Short MWCNTs vs. Long MWCNTs	<i>P</i> > 0.05	<i>P</i> < 0.001	<i>P</i> < 0.001
Short MWCNTs vs. C60 Fullerene	<i>P</i> < 0.001	<i>P</i> < 0.001	<i>P</i> < 0.001
Short MWCNTs vs. Fullerene Soot	<i>P</i> < 0.001	<i>P</i> < 0.001	<i>P</i> < 0.001
Long MWCNTs vs. C60 Fullerene	<i>P</i> < 0.001	<i>P</i> < 0.001	<i>P</i> < 0.001
Long MWCNTs vs. Fullerene Soot	<i>P</i> < 0.001	<i>P</i> < 0.001	<i>P</i> < 0.001
C60 Fullerene vs. Fullerene Soot	<i>P</i> < 0.001	<i>P</i> > 0.05	<i>P</i> < 0.001

**Table 2.** Tentative wavenumber assignments for the top five peaks (in order of magnitude) from the cluster vector for *P. fluorescens* treated with 0.01 mg.L<sup>-1</sup> of (A) Short MWCNTs; (B) Long MWCNTs; (C) C<sub>60</sub> Fullerene; and, (D) Fullerene soot.

**A.**

Short MWCNTs	
Wavenumber (cm <sup>-1</sup> )	Assignment
1065	C-O stretching of DNA
1084	$\nu_s\text{PO}_2^-$
1666	Amide I
1516	Amide II
1794	Lipid

**B.**

Long MWCNTs	
Wavenumber (cm <sup>-1</sup> )	Assignment
1080	$\nu_s\text{PO}_2^-$
1782	Lipid
1142	C-O stretching of carbohydrate
1516	Amide II
1501	Amide II

**C.**

C60 Fullerene	
Wavenumber (cm <sup>-1</sup> )	Assignment
1447	CH3 bending of proteins
1639	Amide I
1501	Amide II
1574	Amide II
1115	Carbohydrate

**D.**

Fullerene soot	
Wavenumber (cm <sup>-1</sup> )	Assignment
1084	$\nu_s\text{PO}_2^-$
1072	C-O vibration of DNA
1516	Amide II
1782	Lipid
1219	$\nu_{as}\text{PO}_2^-$

**Table 3.** Tentative wavenumber assignments for the top five peaks (in order of magnitude) from the cluster vector for *M. vanbaalenii* treated with 0.01 mg.L<sup>-1</sup> of **(A)** Short MWCNTs; **(B)** Long MWCNTs; **(C)** C<sub>60</sub> Fullerene; and, **(D)** Fullerene soot.

**A.**

Short MWCNTs	
Wavenumber (cm <sup>-1</sup> )	Assignment
1003	Carbohydrate
1420	Proteins
1435	Proteins
1060	C-O stretching of DNA
937	DNA

**B.**

Long MWCNTs	
Wavenumber (cm <sup>-1</sup> )	Assignment
1555	Amide II
1504	Amide II
1130	C-O stretching of carbohydrate
934	DNA
1466	Amide II

**C.**

C60 Fullerene	
Wavenumber (cm <sup>-1</sup> )	Assignment
1385	COO <sup>-</sup> stretching
1018	CO vibration of polysaccharides
1003	Carbohydrate
1234	$\nu_{as}PO_2^-$
1053	C-O stretching and C-O bending of carbohydrate

**D.**

Fullerene soot	
Wavenumber (cm <sup>-1</sup> )	Assignment
1003	Carbohydrate
1720	C=O stretching of lipid
1558	Amide II
1015	CO vibration of polysaccharides
1466	Amide II

**Table 4.** Tentative wavenumber assignments for the top five peaks (in order of magnitude) of positive control (UV-A exposed) for (A) *P. fluorescens*; and, (B) *M. vanbaalenii* cells with unpaired *t*-tests to show significance.

**A.**

<i>P. fluorescens</i> treated with 45 minute UV-A	
Wavenumber (cm <sup>-1</sup> )	Assignment
1717	C=O stretching of lipid
1747	C=C vibration of lipids
1697	Amide I
1682	Amide I
1732	Fatty acids

Unpaired <i>t</i> -test - UV-A treated <i>P. fluorescens</i>	
<i>P</i> -value	<i>P</i> < 0.0001
Are means signif. different? ( <i>P</i> < 0.05)	Yes
One- or two-tailed <i>P</i> -value?	Two-tailed

**B.**

<i>M. vanbaalenii</i> treated with 45 minute UV-A	
Wavenumber (cm <sup>-1</sup> )	Assignment
1717	C=O stretching of lipid
1747	C=C vibration of lipids
1697	Amide I
1682	Amide I
1732	Fatty acids

Unpaired <i>t</i> -test: UV-A-treated <i>M. vanbaalenii</i>	
<i>P</i> -value	<i>P</i> < 0.0001
Are means signif. different? ( <i>P</i> < 0.05)	Yes
One- or two-tailed <i>P</i> -value?	Two-tailed